

## Improving the Jason-1 Ground Retracking to Better Account for Attitude Effects

L. AMAROUCHE , P. THIBAUT , O. Z. ZANIFE , J.-P. DUMONT , P. VINCENT & N. STEUNOU

To cite this article: L. AMAROUCHE , P. THIBAUT , O. Z. ZANIFE , J.-P. DUMONT , P. VINCENT & N. STEUNOU (2004) Improving the Jason-1 Ground Retracking to Better Account for Attitude Effects, *Marine Geodesy*, 27:1-2, 171-197, DOI: [10.1080/01490410490465210](https://doi.org/10.1080/01490410490465210)

To link to this article: <http://dx.doi.org/10.1080/01490410490465210>



Published online: 12 Aug 2010.



Submit your article to this journal 



Article views: 209



View related articles 



Citing articles: 63 View citing articles 

Full Terms & Conditions of access and use can be found at  
<http://www.tandfonline.com/action/journalInformation?journalCode=umgd20>

# Improving the Jason-1 Ground Retracking to Better Account for Attitude Effects

L. AMAROUCHE

P. THIBAUT

O. Z. ZANIFE

J.-P. DUMONT

Collecte Localisation Satellite (CLS)

Ramonville Saint-Agne, France

P. VINCENT

N. STEUNOU

Centre National d'Etudes Spatiales (CNES)

Toulouse, France

*After two years of verification and validation activities of the Jason-1 altimeter data, it appears that all the mission specifications are completely fulfilled. Performances of all instruments embarked onboard the platform meet all the requirements of the mission. However, the star tracker system has shown some occasional abnormal behavior leading to mispointing angles out of the range of Jason-1 system specification which states that the altimeter antenna shall be pointed to the nadir direction with an accuracy below 0.2 degree (3 sigma). This article discusses the platform attitude angle and its consequences on the altimetric estimates. We propose improvements of the Jason-1 retracking process to better account for attitude effects.*

*The first star tracker anomalies for the Jason-1 mission were detected in April 2002. The Poseidon-2 algorithms were specified assuming an antenna off-nadir angle smaller than 0.3 degree. For higher values, the current method to estimate the ocean parameters is known to be inaccurate. Thus, the algorithm has to be reviewed, and more specifically, the present altimeter echo model has to be modified to meet the desired instrument performance.*

*Therefore, we derive a second order analytical model of the altimeter echo to take into account attitude angles up to 0.8 degree, and consequently, we adapt the retracking algorithm. This new model is tested on theoretical simulated data using a maximum likelihood estimation. Biases and noise performance characteristics are computed for the different estimated parameters. They are compared to the ones obtained with the current algorithm. This new method provides highly improved estimations for high attitude angles. It is statistically validated on real data by applying it on several cycles of Poseidon-2 raw measurements. The results are found to be consistent with those obtained from simulations. They also fully agree with the TOPEX estimates when*

Received 1 December 2003; accepted 28 January 2004.

The authors are thankful for the constructive comments from E. Rodriguez and the anonymous reviewer. This work is supported by the Centre National d'Etudes Spatiales. It has been accomplished thanks to the help and expertise of the Jason CAL/VAL team in CLS, which provided us with some of their processing chains and internal validation results. We also gratefully acknowledge the SSALTO exploitation team in CLS which provided us with the operational and reprocessed products. Last, the authors would like to thank G. Born who has made possible the publication of this article in the volume of *Marine Geodesy* dedicated to the Jason-1 mission.

Address correspondence to L. Amarouche, Collecte Localisation Satellite (CLS), 8–10, Rue Hermès, Ramonville Saint-Agne 31526, France. E-mail: laiba.amarouche@cls.fr

flying along the same ground track. Finally, the estimates are also in agreement with the ones available in the current I/GDR (Intermediate Geophysical Data Record) products when mispointing lies in the mission specifications.

**Keywords** Jason-1, Poseidon-2, retracking, echo model, mispointing

The Jason-1 satellite was successfully launched on 7 December 2001 to insure the continuity of the oceanographic observations provided by the TOPEX/Poseidon mission which began in 1992 (Menard et al. 2003). The payload of Jason-1 is described extensively in Perbos et al. (2003). A brief overview is provided here:

- A dual-frequency radar altimeter (Ku and C bands): Poseidon-2;
- A three-channel radiometer: JMR (Jason Microwave Radiometer);
- Two dual-frequency tracking systems: DORIS (Détermination d'Orbite et Radiopositionnement Intégré par Satellite) and GPS (Global Positioning System) receivers;
- A laser retro reflector array.

During the first two years of the Jason-1 mission, some occasional abnormal behavior of the star trackers system were observed, leading to platform off-nadir angle values out of the Jason-1 system specification which states that the altimeter shall be pointed to the nadir direction with an accuracy below 0.2 degree (3 sigma). All Poseidon-2 algorithms were specified assuming an antenna mispointing angle smaller than 0.3°. On 4 April 2002, high values of the mispointing angle were observed (see Figure 1). Figure 2 gives the percentage of mispointing values greater than 0.2 degree, from October 2002 to January 2004. Two periods displaying high mispointing angles are observed: December 2002 (cycles 35 and 36 which are studied here) and February 2003 (cycle 41). For these two periods, less than 5% of the data is affected. A peak is observed in the second half of November 2003. However, it is not meaningful, as it corresponds to a period when the Jason-1 satellite was in a safehold mode. To process data acquired in such circumstances, modifications of the retracking algorithm had to be considered to take into account higher values of the mispointing angle.

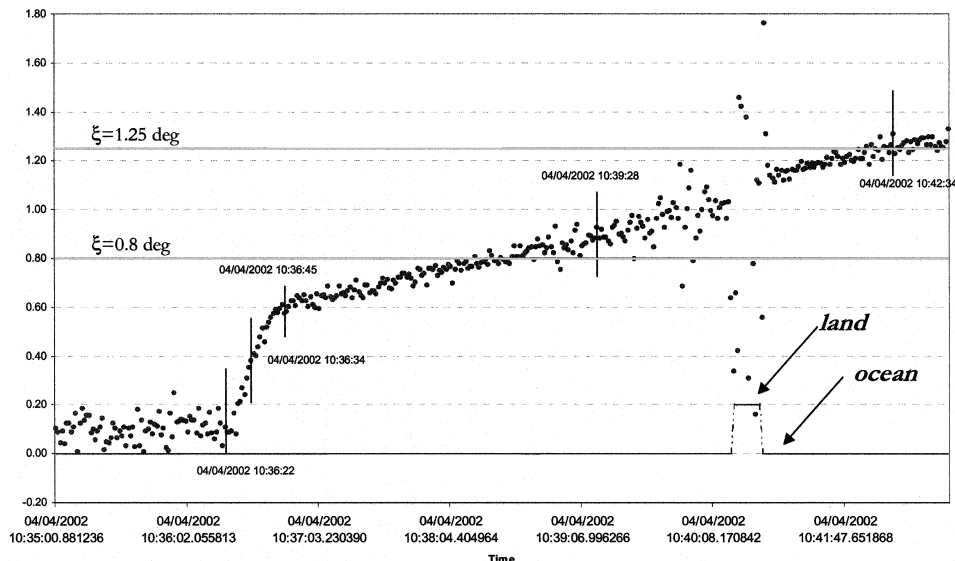


**FIGURE 1** Attitude angle ( $\xi$ ) of Jason-1 platform during the first star tracker incident 04/04/2002.

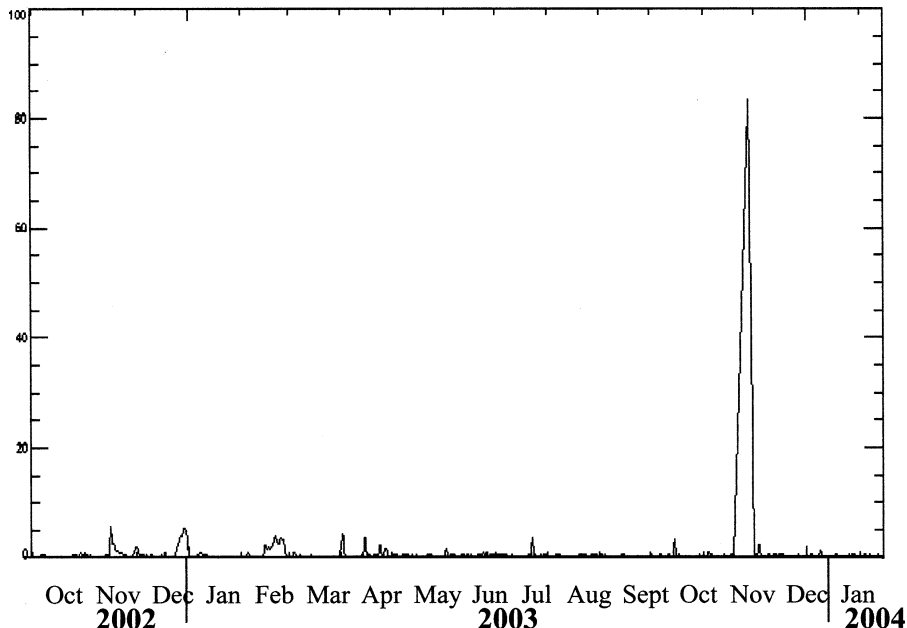


**FIGURE 2** Percentage of time when the off nadir angle is greater than 0.2 degree.

For this purpose, a new analytical expression of the radar echo model is proposed and validated.

It is worth adding that a potential further degradation of the star tracker could lead to modifications of the present strategy consisting of maintaining the attitude within the specifications. Indeed, the attitude orbit control system (AOCS) could be used in such a way that mispointing should be free to vary up to 0.5 degree. In such a case, the algorithm improvements discussed in herein are required. Note that in this article, we are dealing only with the Ku band.

The next section is a brief review of the current Poseidon-2 ground retracking algorithm. In particular, a short description of Poseidon-2 altimeter characteristics is given along with a review of the first order echo model and the estimation method used to derive the ocean parameters. In the following section, a new analytical expression of the waveform which includes the addition of higher order terms is derived. Next, this new formulation is evaluated and biases and noises on the estimated parameters are computed theoretically using simulated data. The next section presents the results when the improved model is applied to real raw Poseidon-2 data. The last section provides the conclusions of this work and some perspectives to further improve the Jason-1 retracking procedure.

### Jason-1 Ground Retracking Algorithm in GDRs

This section gives a general description of the Jason-1 ground retracking algorithm as operationally used to derive Jason-1 I/GDR products. The Poseidon-2 altimeter characteristics are summarized. Then, the ground retracking algorithm used to estimate the ocean parameters is presented along with the method used to estimate the attitude angle.

#### *Poseidon-2 Altimeter General Description*

The Poseidon-2 altimeter characteristics have been described extensively by Carayon et al. (2003). A brief review is provided here. The Poseidon-2 altimeter transmits 105.6  $\mu$ s

duration pulses at a frequency of 13.575 GHz for the Ku band (5.3 GHz for the C band). These pulses are frequency linear modulated and then transmitted towards the ocean surface at a pulse repetition frequency (PRF) equal to  $2060 \text{ Hz} \pm 10\%$  (1800 Hz for the Ku band and 260 Hz for the C band). After reflection from the surface, the pulses are received back on board and mixed with an emitted pulse (Chelton et al. 1989). The resulting individual echo consists of 128 samples separated by 3.125 ns (or equivalently, 46.8 cm or 9469 Hz). In order to reduce the statistical fluctuations (speckle) which affect the individual echoes and to perform real time tracking, these echoes are averaged on-board over a period (instrument cycle) of about 50 ms. The resulting signal is processed by the on-board tracking to derive the range and the power which will be used as a priori parameters during the next instrument cycle. The tracking function consists of keeping the waveforms well centered in range and power in the analysis window. This is performed thanks to first and second order filter tracker closed loops (Zanifé et al. 2003). An onboard Maximum Likelihood Estimator (MLE) algorithm is then applied to these waveforms to derive the ocean parameters. These estimates are used to derive the real time OSDR (Operational Sensor Data Record) products (Desai and Vincent 2003). A ground retracking is also applied. Its main purpose is to refine these estimates in order to get the most accurate ocean parameters.

### ***The First Order Echo Model***

Moore and Williams (1957), Barrick (1972) and Barrick and Lipa (1985) demonstrated that for a rough scattering surface, the average return power as a function of delay ( $t$ ) could be expressed as a convolution of three terms:

$$W(t) = \text{FSSR}(t) * \text{PTR}(t) * \text{PDF}(t), \quad (1)$$

where:

FSSR is the flat sea surface response,

PTR is the radar point target response, and

PDF is the surface elevation probability density function of specular points.

This study makes the usual assumption that the specular points density function is identical to the geometric surface heights density function. Any difference between these two functions enters in the Electromagnetic Bias theory (Yaplee et al. 1971) and does not concern our study. In the development below, we also assume that the PDF function is a Gaussian one.

The theoretical radar point target response is expressed as:

$$\text{PTR}(t) = \left| \frac{\sin(\pi B t)}{\pi B t} \right|^2, \quad (2)$$

where  $B$  is the reception bandwidth of the altimeter.

To perform the convolution of the three terms, the PTR function is approximated by a Gaussian function:

$$\text{PTR}(t) \approx \exp \left( \frac{-t^2}{2\sigma_p^2} \right); \quad (3)$$

$\sigma_p$  is the standard deviation of the Gaussian function that models the PTR. Barrick (1972) and Brown (1977) used  $\sigma_p = \frac{1}{2\sqrt{2\ln 2}}r_t \approx 0.425.r_t$ , with  $r_t$  being the time resolution.

MacArthur (1978) suggested that  $\sigma_p = 0.513 r_t$  is a good enough approximation of  $\sigma_p$ . Amarouche et al. (2001a and 2001b), studied the effects of the PTR Gaussian approximation on the estimated ocean parameters and found that, due to the symmetrical shape of the Poseidon-2 true (measured) PTR (Carayon et al. 2003), the only parameter affected by this approximation was the significant wave height (SWH). In the current Poseidon-2 ground retracking algorithm, the value of  $\sigma_p$  is then kept constant ( $0.513 r_t$ ), and the biased estimates of SWH are corrected using look-up tables. These look-up tables are built using a Poseidon-2 altimeter simulator which inputs the true (measured) PTR to simulate the altimeter waveforms. The ground retracking estimator is then applied to these simulated echoes to derive the resulting biases on the estimated parameters.

Here, we are particularly interested in the FSSR function due to its dependency on the antenna mispointing angle. This function was derived by Brown (1977) and is expressed as:

$$\text{FSSR}(t) = A \exp(-\delta t) U(t) \sum_{k=0}^{\infty} \frac{(-1)^k \Gamma(k + 1/2)}{\sqrt{\pi} \Gamma(k + 1)} \left[ \frac{\gamma \beta t^{1/2}}{8 \cos^2 \xi} \right]^k I_k(\beta t^{1/2}), \quad (4)$$

where the  $I_k$  are the modified Bessel functions of the second kind, and

$$\delta = \frac{4}{\gamma} \frac{c}{h} \cos(2\xi), \quad \text{and} \quad (5)$$

$$\beta = \frac{4}{\gamma} \left[ \frac{c}{h} \right]^{1/2} \sin(2\xi). \quad (6)$$

$U(t)$  is a unit step function,  $c$  is the speed of light,  $\xi$  is the off-nadir pointing angle and  $h$  is the modified satellite altitude given by:

$$h = H \left( 1 + \frac{H}{R_t} \right), \quad (7)$$

where  $H$  is the satellite altitude and  $R_t$  is the radius of the Earth.

$\gamma$  is an antenna beamwidth parameter given by  $\gamma = 1/2 \ln 2 \sin^2 \theta_{-3\text{dB}}$ ,  $\theta_{-3\text{dB}}$  being the half-power antenna beamwidth. The amplitude term  $A$  is related to  $\gamma$  and  $\xi$  by:

$$A = A_0 \exp \left[ -\frac{4}{\gamma} \sin^2 \xi \right], \quad (8)$$

$A_0$  containing several constants related to the instrument characteristics and to the propagation losses.

Brown (1977) demonstrated that the zero order term of the infinite series of Equation (4) is enough to provide a very good approximation of the FSSR. Indeed, the higher order terms are negligible (for  $\xi < 1^\circ$ ) because:

$$\frac{\gamma \beta t^{1/2}}{8 \cos^2 \xi} \ll 1. \quad (9)$$

Equation (4) can then be read:

$$\text{FSSR}(t) = A \exp(-\delta t) I_0(\beta t^{1/2}) U(t). \quad (10)$$

Following Abramowitz and Stegun (1964), the zero order term of the Bessel function expansion  $I_0$  is given by:

$$I_0(z) = \sum_{n=0} \left( \frac{z^2}{4} \right)^n \left( \frac{1}{n!} \right)^2, \quad \text{with } z = \beta t^{1/2}. \quad (11)$$

Considering that  $\xi$  is smaller than  $0.3^\circ$ , Rodriguez (1988) used only the first two terms ( $n = 0, 1$ ) to develop  $I_0$ .  $I_0$  could then be written using the exponential function as:

$$I_0(\beta t^2) \approx e^{\frac{\beta^2 t}{4}}. \quad (12)$$

After substituting (12) in (10), FSSR can then read:

$$\text{FSSR}(t) = 2A \exp \left[ -\left( \delta - \frac{\beta^2}{4} \right) t \right] U(t). \quad (13)$$

Using Equation (13) and computing the convolution as in Equation (1), the resulting average return power is then given by:

$$W(t) = A \exp(-v)[1 + \text{erf}(u)], \quad (14)$$

with

$$u = \frac{t - \alpha \sigma_c^2}{\sqrt{2} \sigma_c}, \quad v = \alpha \left( t - \frac{\alpha}{2} \sigma_c^2 \right), \quad \text{and} \quad \alpha = \delta - \beta^2/4; \quad (15)$$

$\sigma_c$  is a parameter related to the standard deviation of the ocean heights  $\sigma_s$  and to  $\sigma_p$  (see Equation (3)) according to:

$$\sigma_c^2 = \sigma_p^2 + \sigma_s^2. \quad (16)$$

The analytical ocean return model was refined by Hayne (1980) who considered higher order moments of the PDF function in Equation (1). In particular, a third order moment of the ocean heights (skewness) was included.

However, this analytical form is still valid only for pointing angles smaller than  $0.3^\circ$ . As the purpose here is to consider higher mispointing angles, a higher order term of the Bessel function expansion will have to be used.

### **Description of the Ground Retracking Procedure**

The theoretical shape of a radar echo over an ocean surface is represented in Figure 3. The different ocean parameters derived from this echo are as follows.

- The epoch  $\tau$ , defined as the position of the signal in the analysis window with respect to the tracking reference point. The precise range estimate will be derived from both the tracking range and the epoch  $\tau$  estimates.
- The amplitude  $P_u$  of the waveform which is used to derive the backscatter coefficient  $\sigma_0$ . This latter is related to ocean surface wind speed.

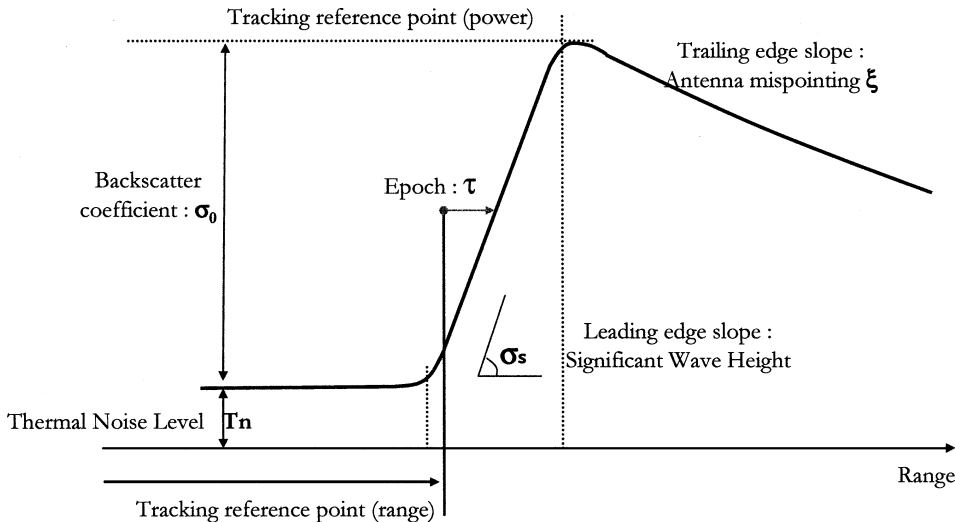


**FIGURE 3** Theoretical shape of the altimeter echo and the corresponding ocean parameters.

- The slope of the leading edge, which is a function of the standard deviation of the sea surface heights  $\sigma_s$  and related to the significant wave height ( $\text{SWH} = 4\sigma_s$  when assuming a Gaussian distribution of ocean heights).
- The thermal noise level  $T_n$ .
- The off-nadir angle  $\xi$  that is linked to the trailing edge slope.

The retracking process consists of the estimation of  $\tau$ ,  $P_u$ , and  $\sigma_c$  (and then SWH). These estimates are performed making the measured waveform coincide with a return power model according to unweighted Least Square Estimators derived from Maximum Likelihood Estimators (Dumont 1985; Rodriguez 1988). An unweighted estimator is used instead of a weighted estimator to ensure the robustness of the estimates.

Assuming that the waveform samples are completely decorrelated for different samples and for different pulses, an iterative solution is obtained by developing the total cost function in a Taylor series at the first order from an initial set of estimates. Note that the pulse-to-pulse decorrelation assumption is true (Walsh 1982; Rodriguez et al. 1994; Amarouche 2001a) for the Poseidon-2 PRF, except for very low sea state conditions (SWH smaller than 1 meter) which are unusual. The estimated parameters are expressed as (Dumont 1985; Zanifé et al. 2003):

$$\theta_{m,n} = \theta_{m,n-1} - g(BB_T)_{\theta_{m,n}}^{-1}(BD)_{\theta_{m,n-1}} \quad (17)$$

where  $\theta_{m,n}$  is the estimated parameter at iteration  $n$ ,  $m$  is the index of the estimated parameter and  $g$  the loop gain (between 0 and 1). The matrix of unweighted partial derivatives,  $B$ , and the vector of unweighted differences,  $D$ , are given by:

$$B_{m,k} = \frac{1}{P_u} \frac{\partial \bar{V}_k}{\partial \theta_m} \quad \text{and} \quad D_{k,1} = \frac{\bar{V}_k - V_k}{P_u} \quad (18)$$

with  $k$  the sample index,  $\bar{V}_k$  the model waveform sample  $k$ ,  $V_k$  the measured waveform sample  $k$  and  $P_u$  the estimated power.

The convergence criterion is based on the merit function  $\chi^2$  or MQE (Mean Quadratic Error) defined by:

$$\chi^2 = \sum_i \left( \frac{V_{i-}Vm_i}{Pu} \right)^2. \quad (19)$$

The iterative procedure is considered to be stable if the differences of the values obtained are under a threshold during three consecutive iterative steps.

In the next sections, this algorithm will be called MLEN, N being the number of the retrieved parameters.

### **Present Method to Estimate the Attitude Angle**

The use of a MLE3 algorithm to solve for range,  $\sigma_c$  and  $\sigma_0$  as outputs assumes that the mispointing angle is zero. When this is not the case, the mispointing angle should be estimated first and then taken into account (after smoothing over 30 seconds) in the echo model used in the MLE3.

When mispointing exists, the slope of the trailing edge of the echo is modified. That is why this slope is presently used for this estimation. In this region, the analytical expression of the waveform given by the Equation (14) can be simplified (using the fact that  $\text{erf}(x)$  is equal to 1 in the trailing edge region). It comes:

$$W(t) \approx 2A \exp(-v). \quad (20)$$

If we note  $X = \xi^2$  and considering that  $|X| \ll 1$ , the slope of the trailing edge of the logarithm of the waveform can be expressed as:

$$\text{Slope} = -\alpha T \left[ 1 - \left( 2 + \frac{4}{\gamma} \right) X \right]. \quad (21)$$

If  $\hat{s}$  is the estimated value of this slope, using a linear regression on the trailing edge, the estimated value of  $X$  is

$$\hat{X} = \frac{\gamma}{2(\gamma + 2)} \left[ 1 + \frac{\hat{s}}{\alpha T} \right]. \quad (22)$$

### **Second Order Model of the Altimeter Waveform**

In this section, the purpose is to derive a new analytical model of the altimeter waveform taking into account mispointing values higher than  $0.3^\circ$ . The Bessel function (Equation (11)) in the FSSR function was developed for mispointing angles up to  $0.3^\circ$ . To consider angle values up to  $1^\circ$ , a higher order has to be used. In all the equations below, notations are the same as in the section on the first order echo model.

The  $I_0$  Bessel function developed to order 2 can be written as:

$$I_0(z) = \sum_{n=0} \left( \frac{z^2}{4} \right)^n \left( \frac{1}{n!} \right)^2 \approx 1 + \frac{z^2}{4} + \frac{z^4}{64}. \quad (23)$$

It can also be expressed as

$$I_0(z) \approx 2 \left[ 1 + \frac{z^2}{8} + \frac{z^4}{128} \right] - 1 = 2 \left[ 1 + \frac{z^2}{8} + \frac{1}{2} \left( \frac{z^2}{8} \right)^2 \right] - 1. \quad (24)$$

Using the Taylor series of the exponential function at the second order,  $I_0$  becomes

$$I_0(\beta t^{1/2}) \approx 2e^{\frac{\beta^2 t}{8}} - 1. \quad (25)$$

Substituting Equation (25) in Equation (10) yields

$$\text{FSSR}(t) = 2A \exp \left[ -\left( \delta - \frac{\beta^2}{8} \right) t \right] U(t) - A \exp[-\delta t] U(t) \quad (26)$$

This function is the sum of two terms, each being analogous to the right hand side of Equation (13). After performing convolution and considering the fact that the convolution is linear, the altimeter received power can then be expressed as

$$W(t) = A \exp(-v_1)[1 + \text{erf}(u_1)] - \frac{A}{2} \exp(-v_2)[1 + \text{erf}(u_2)], \quad (27)$$

with

$$u_1 = \frac{t - \alpha_1 \sigma_c^2}{\sqrt{2} \sigma_c}, \quad v_1 = \alpha_1 \left( t - \frac{\alpha_1}{2} \sigma_c^2 \right), \quad \alpha_1 = \delta - \beta^2/8, \quad (28)$$

$$u_2 = \frac{t - \alpha_2 \sigma_c^2}{\sqrt{2} \sigma_c}, \quad v_2 = \alpha_2 \left( t - \frac{\alpha_2}{2} \sigma_c^2 \right), \quad \text{and} \quad \alpha_2 = \delta. \quad (29)$$

The right hand side of Equation (27) is the sum of two terms, each being analogous to the main term of the first order echo model (Equation (14)). In the same way, a second order echo model using a skewness coefficient of ocean wave heights can easily be derived (not shown in this study).

Figure 4 displays the shape of the echo obtained using: (a) the first order model (Equation (14)), (b) the new second order model (Equation (27)) and, (c) the three-term convolution of Equation (1) using a complete Bessel function in the FSSR expression (Equation (10)) considered as the reference. We used a high mispointing angle value ( $0.7^\circ$ ): The second order model better fits the complete model.

We generated echoes with mispointing angles from 0 to 1 degree using the three-term convolution with the FSSR function based on the complete Bessel function and a complete sinc function for the altimeter PTR. Two different estimation methods were then applied to these echoes to retrieve the mispointing angle. The first method is the one presently used in the ground processing and as described above. The second method is based on a Maximum Likelihood Estimator using the second order model of Equation (27) and solving for two parameters: the echo power and the square of the mispointing angle. In that case, the MLE algorithm is applied on the trailing edge part of the echo only. The results are presented in Figure 5. For small mispointing angle values, the two models are fully equivalent. For high angle values, the second order model is much more efficient because of the large biases associated with the current method. Note that the second order model is valid up to approximately  $0.8^\circ$ .

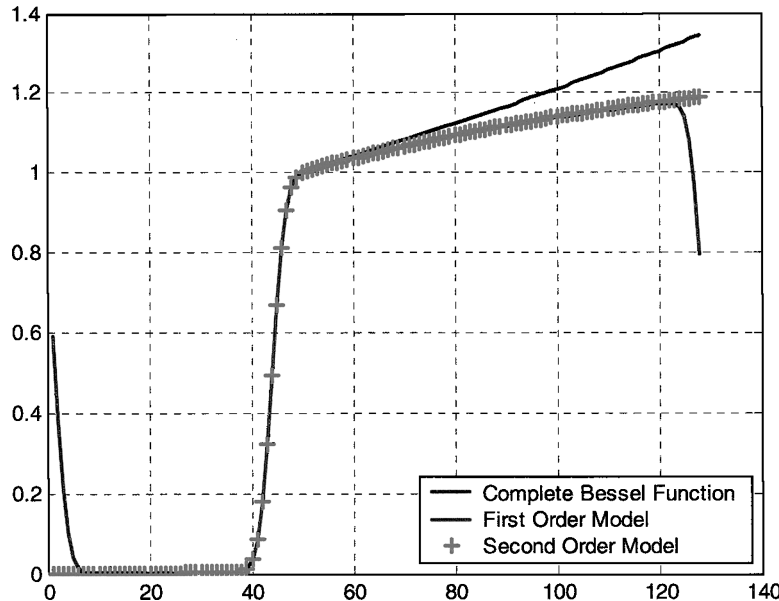


**FIGURE 4** Comparison of three echo models for a mispointing angle of  $0.7^\circ$ : convolution with the complete Bessel function (-), the first order model (---) and the second order model (+).

### Theoretical Performance

The purpose of this section is to propose an algorithm able to derive geophysical parameters with the best possible accuracy, fully taking into account all the effects of mispointing in the solution process. Several methods using the previously described echo model (Equation (27)) were tested and compared. It is not the goal here to discuss all methods: Numerous

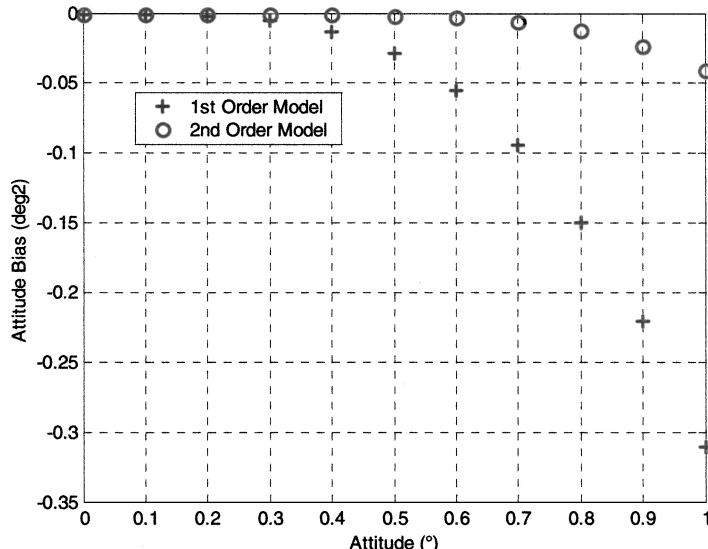


**FIGURE 5** Comparison of mispointing angle estimates using the first order model (+) and the second order model (o).

tests led us to choose an MLE4 estimator with the range, SWH,  $\sigma_0$  and  $\xi^2$  as unknowns.  $\xi^2$  is used instead of  $\xi$  because  $\xi^2$  is the quantity which appears in the model (also, the use of the square root of  $\xi^2$  results in a singular behavior of the derivatives around  $\xi = 0$ ). In the following, the performance of this algorithm will be compared to the current MLE3 method used in the Poseidon-2 altimeter ground processing.

To simulate the estimation process, altimeter waveforms were generated using the three-term convolution with a complete Bessel function in the FSSR function (Equation (4)) and a sinc function for the radar PTR (Equation (2)). Each waveform represents the Poseidon-2 raw telemetry Ku-band waveform. It consists of the average of 90 pulses with a PRF of 1800 Hz (equivalent to about 50 ms duration). To simulate the speckle noise, a Gaussian noise was added to each waveform. The variance of this Gaussian noise was set equal to the mean waveform value divided by the number of independent pulses. For the Poseidon-2 PRF, the number of independent pulses is equal to the number of averaged pulses (Walsh 1982; Rodriguez et al. 1994; Amarouche 2001a). These two numbers differ only for very low sea state conditions (SWH smaller than 1 m) and only in the leading edge region.

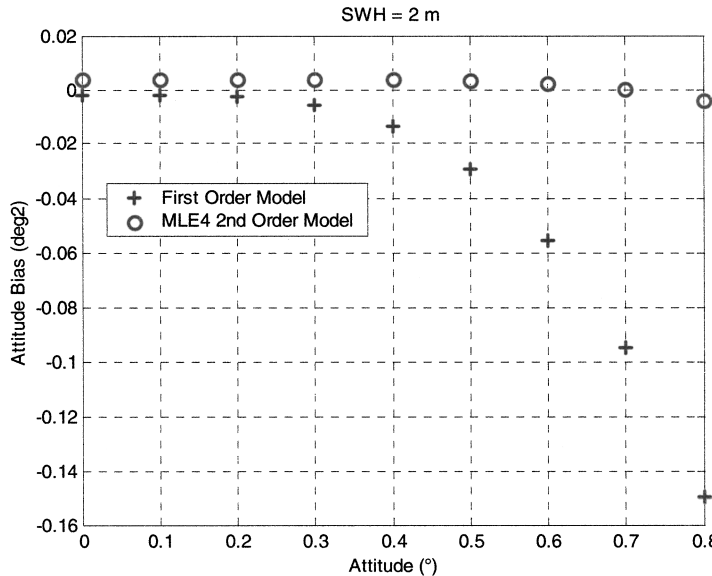
Simulations were computed for a variety of SWH and attitude values respectively ranging between 1 and 8 meters and, 0 and 0.8 degree. After some tests, the 1000 s duration was found to be statistically significant to derive the results that are presented hereafter. Tests were based on twin experiments using MLE4 with the second order model on one hand and the current method of the ground processing (MLE3 with the first order model) on the other hand. The noisy estimated parameters were averaged over 1 s to compute the 1 Hz noise. The bias on these parameters is computed as the difference between the mean of the estimated values and the initial values used to simulate the echoes. In the following, we present the results on the mispointing angle, the range and SWH estimates. For the backscatter coefficient  $\sigma_0$ , simulations showed that the difference between the MLE3 and the MLE4 estimates were not significant (of the order of magnitude of  $10^{-2}$  dB). Comparisons of the  $\sigma_0$  estimates using real Poseidon-2 and TOPEX data will be presented below.

### ***Mispointing Estimation***

Figure 6 illustrates the bias on the estimation of the square of the mispointing angle for a 2 m SWH with respect to the simulated mispointing values. The bias corresponding to the first order model increases with the attitude angle value while the MLE4 bias is approximately constant. The latter is of course, the best situation to be expected. The MLE4 bias is of the order of  $5 \cdot 10^{-3}$  squared degrees. Figure 7 shows the corresponding 1 Hz noise. The noise obtained with the MLE4 is of the order of  $7 \cdot 10^{-3}$  squared degrees which is roughly one half of the noise observed with the current method. For both algorithms, the resulting biases and noises on the estimated mispointing angle are not dependent on the SWH values.

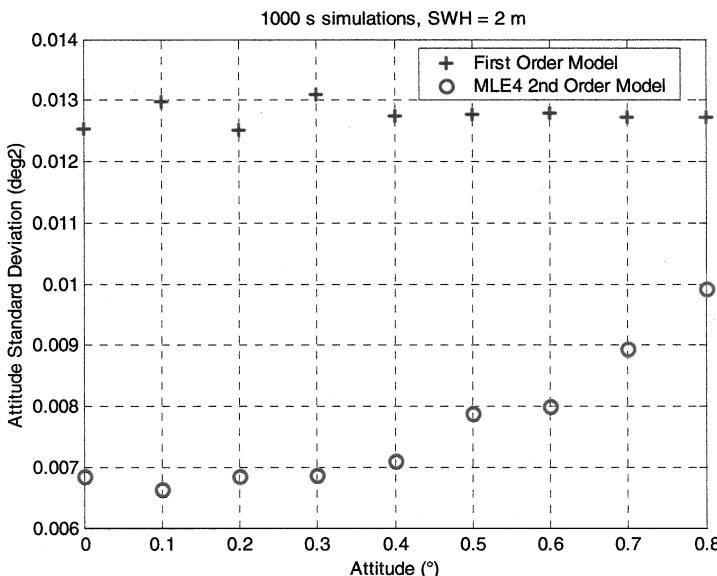
### ***Range Estimation***

Figure 8 (resp. a and b) presents the bias on the range estimates as a function of the simulated mispointing angle  $\xi$ , respectively for SWH = 2 m and SWH = 4 m. As expected, this bias is found to be increasing with the SWH value for both algorithms. The bias associated with the first order echo model is increasing with the mispointing value and reaches high values for high mispointing angles (the range bias is of the order of 6 cm for  $\xi = 0.8^\circ$  and SWH = 2 m). The one associated with the second order model is slightly constant and is very close to zero (it is of the order of magnitude of one millimeter).



**FIGURE 6** Bias on the mispointing estimates using the first order model (+) and using the MLE4 with the second order model (o).

Figure 9 (resp. a and b) displays the corresponding 1 Hz noise on the range estimation for  $\text{SWH} = 2 \text{ m}$  and  $\text{SWH} = 4 \text{ m}$ . As for the bias, the noise is also depending on the  $\text{SWH}$  value for both algorithms and is increasing with it. The noise corresponding to the first order model is a bit smaller than the one obtained with the second order model. However, the maximum difference between the two noise estimates is smaller than 2 millimeters. Such a very small increase of the noise level for the range is thus fully acceptable in order to be able to get accurate estimates even when the off-nadir angle is higher than 0.3 degrees.



**FIGURE 7** 1 Hz noise on the mispointing estimates for  $\text{SWH} = 2$  using the first order model (+) and using the second order model (o).

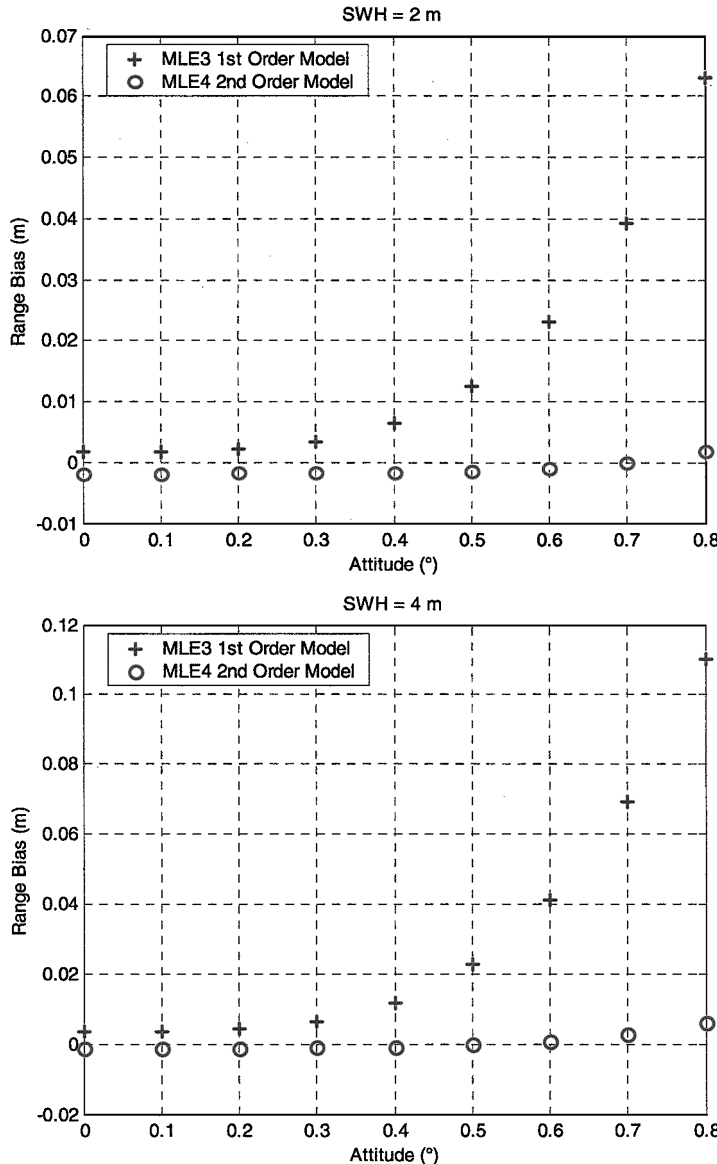


**FIGURE 8** Bias on the range estimates using the first order model (+) and using the second order model (o): (a) SWH = 2 m and (b) SWH = 4 m.

### SWH Estimation

The same types of results are displayed in Figure 10 (resp. a and b) for the significant wave height. The bias on this estimation is found to be proportional to SWH. As for the range estimates, this bias is increasing with SWH. The bias related to the first order echo model is increasing with the mispointing value while the one given by the second order model is approximately constant (with respect to mispointing) and is of the order of 13 cm. This bias is due to the approximation of the radar point target response (PTR) by a Gaussian shape. This PTR effect is corrected for in the ground processing using look up tables.

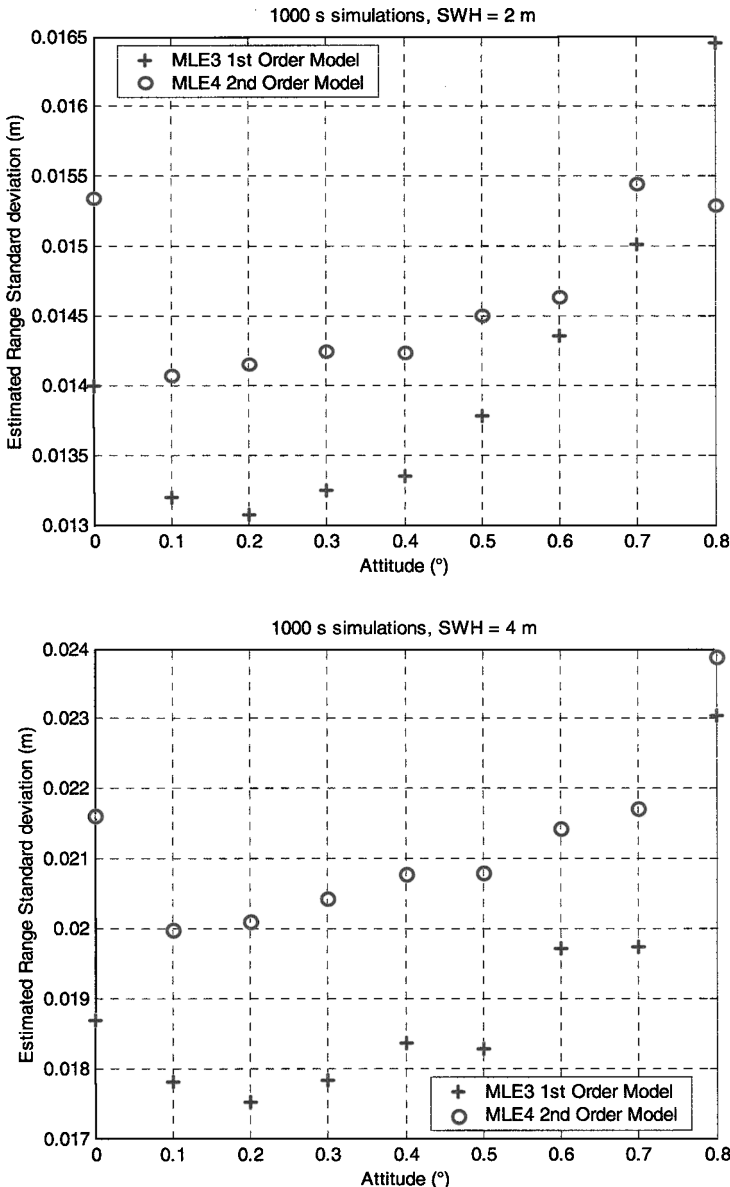


**FIGURE 9** 1 Hz noise on the range estimates using the first order model (+) and using the second order model (o): (a) SWH = 2 m and (b) SWH = 4 m.

Figure 11 (resp. a and b) gives the corresponding 1 Hz noises on these parameters. These noises are dependent on SWH for both algorithms. They have the same order of magnitude for mispointing angles smaller than  $0.4^\circ$ . For higher values, the second order model results in smaller values of noise on the SWH estimate.

## Results Using Real Poseidon-2 Data

The validation of the second order model and the MLE4 retracking algorithm is performed with Poseidon-2 data.

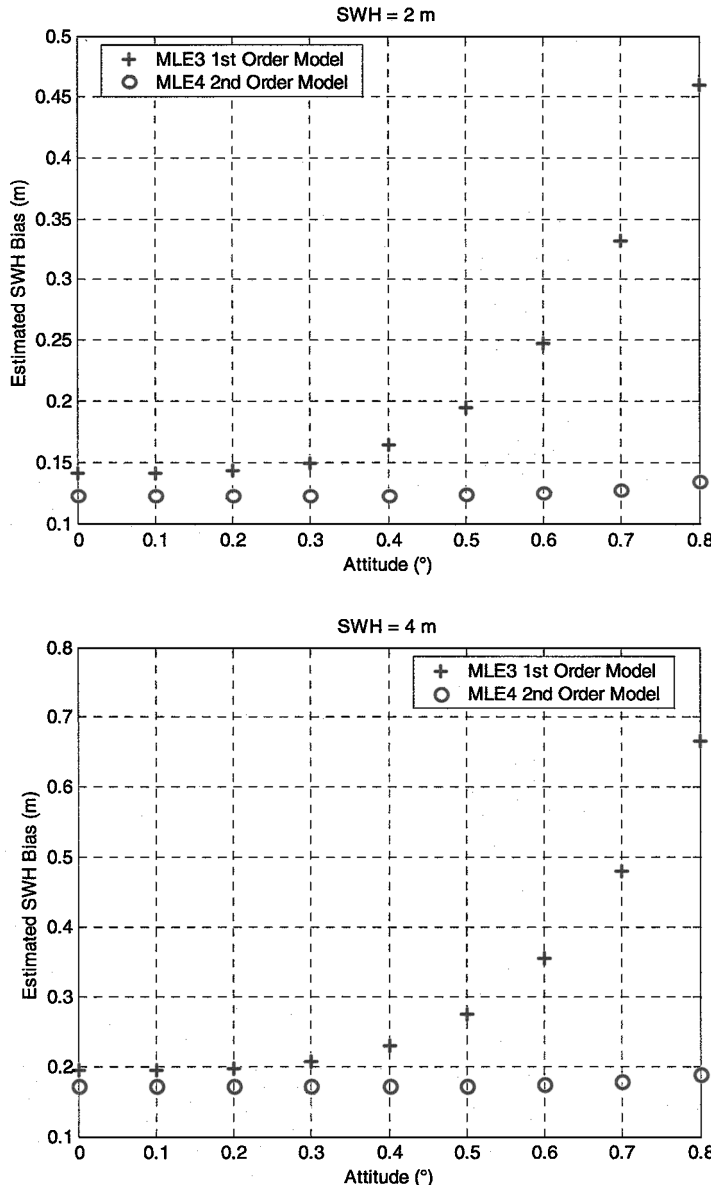


**FIGURE 10** Bias on the significant wave height estimates using the first order model (+) and using the second order model (o): (a) SWH = 2 m and (b) SWH = 4 m.

- In a first step, we will use a small set of real measurements with high mispointing angle values. We will then compare the results to those obtained using the MLE3 algorithm and to TOPEX estimates while flying along the same track.
- In a second step, we will use a whole cycle of data. Retracked data using the second order model will be compared to the MLE3 retracked data found in the current GDR products.

#### *Processing of Data Acquired During the First Star Tracker Incident*

High off-nadir angle values have been observed during the first star tracker incident (Jason-1 STR1) that occurred on 04/04/2002 from 10:36:22 a.m. to 10:40:00 a.m. (latitude varying

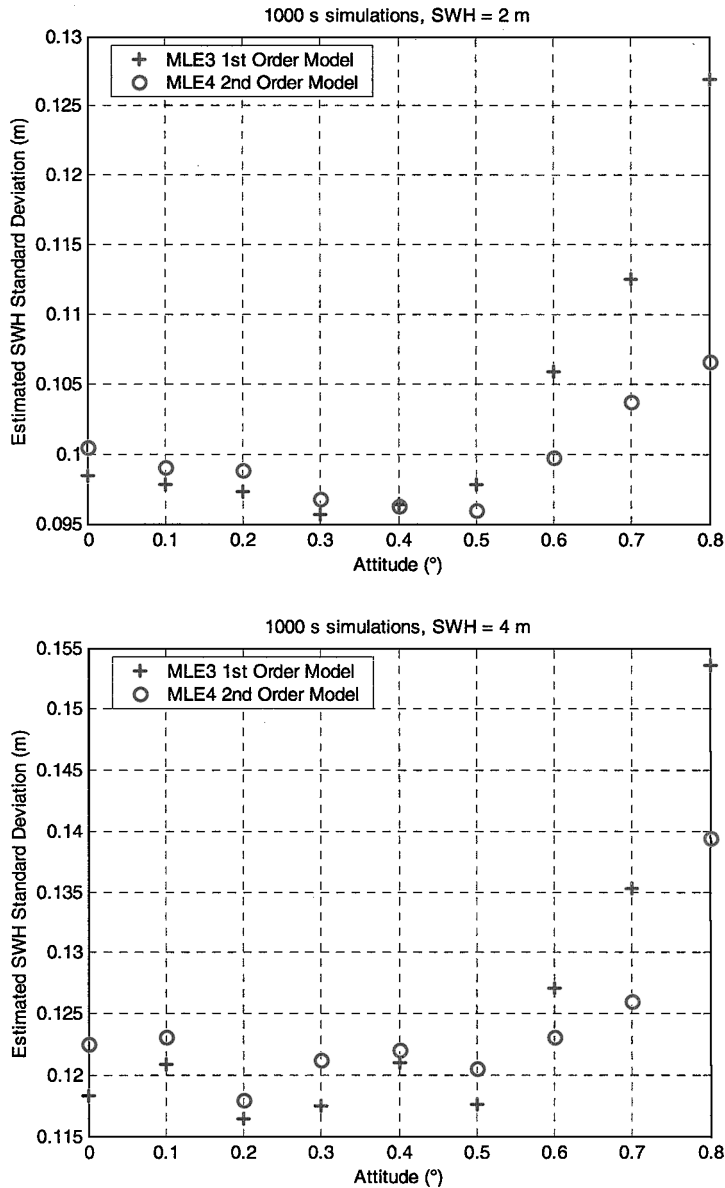


**FIGURE 11** Noise on the significant wave height estimates using the first order model (+) and using the second order model (o): (a) SWH = 2 m and (b) SWH = 4 m.

from +7 deg to -8 deg). The variation of the attitude angle is plotted with respect to latitude in Figure 12 (as the incident occurred during a descending pass (cycle 8, pass 252). Figure 12 has to be read from right to left following decreasing latitudes).

Figures 13 to 15 show the comparison of the significant wave height (SWH), sea surface height residual (SSH\_Res) and backscatter coefficient (Sigma0) obtained with the current MLE3 algorithm (bullets) and the MLE4 algorithm using a second order model (crosses). The corresponding TOPEX measurements (cycle 351, pass 252) are also plotted (triangles). It is important to recall that, during this cycle, TOPEX and Jason-1 were flying on the same ground track with a 73-second time lag separating the two. We can then consider that they

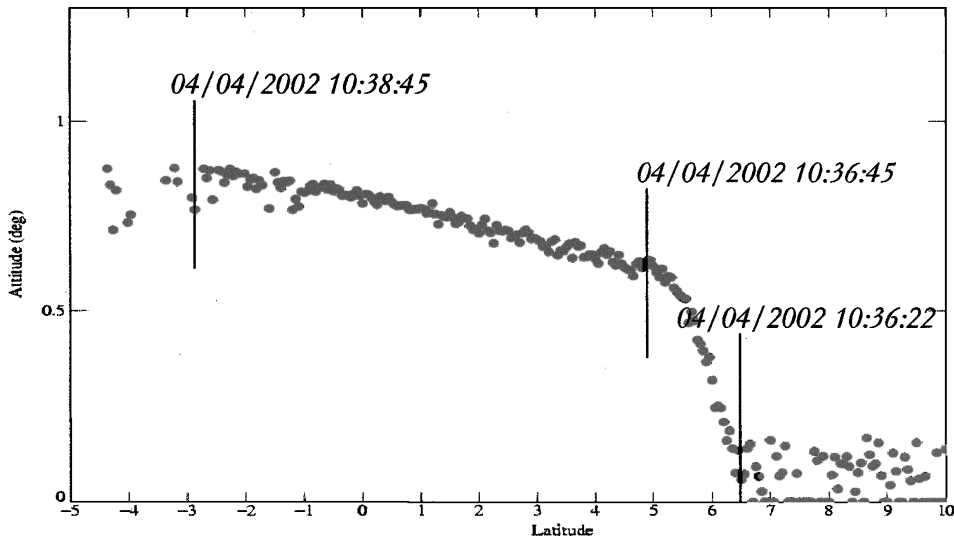


**FIGURE 12** Attitude angle of Jason-1 platform during the first star tracker incident (04/04/2002—Cycle 008 (Jason-1)—pass 252).

observe the same scene. As far as the sigma0 coefficients are concerned (Figures 15a and 15b), both Jason-1 measurements obtained using MLE3 and MLE4 have been shifted by 2.4 dB to be consistent with TOPEX results. In the same way, SSH residuals (Figures 14a and 14b), from MLE3 and MLE4 are shifted by 11 cm to take care of the systematic bias between TOPEX and Poseidon-2 measurements. In agreement with the theoretical

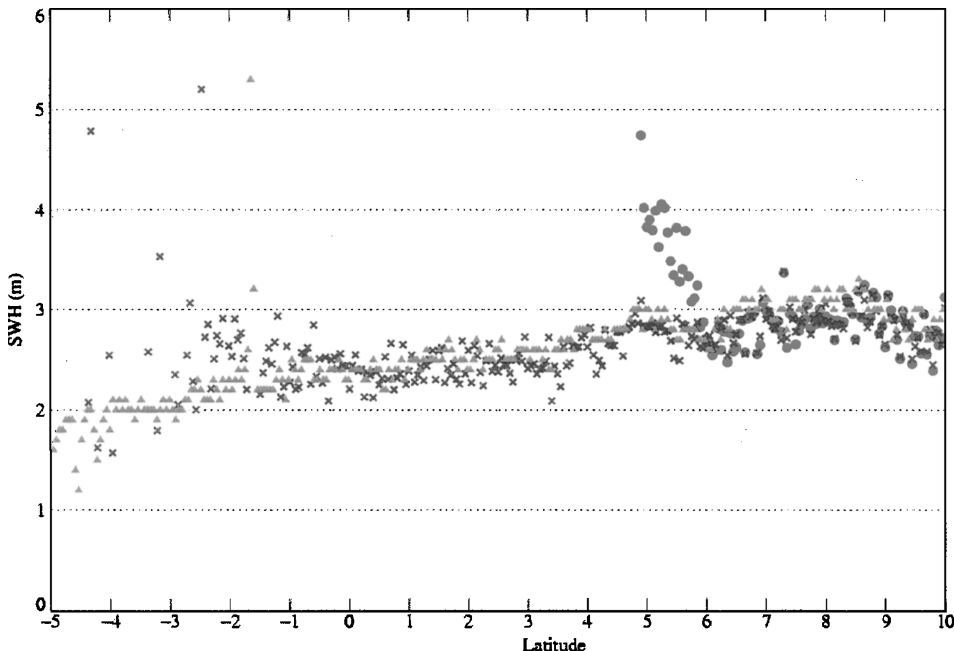


**FIGURE 13a** Significant wave height: MLE3 (bullets), MLE4 (crosses) and Topex (triangles) (first star tracker incident: 04/04/2002—Cycle 008 (Jason-1)—pass 252).

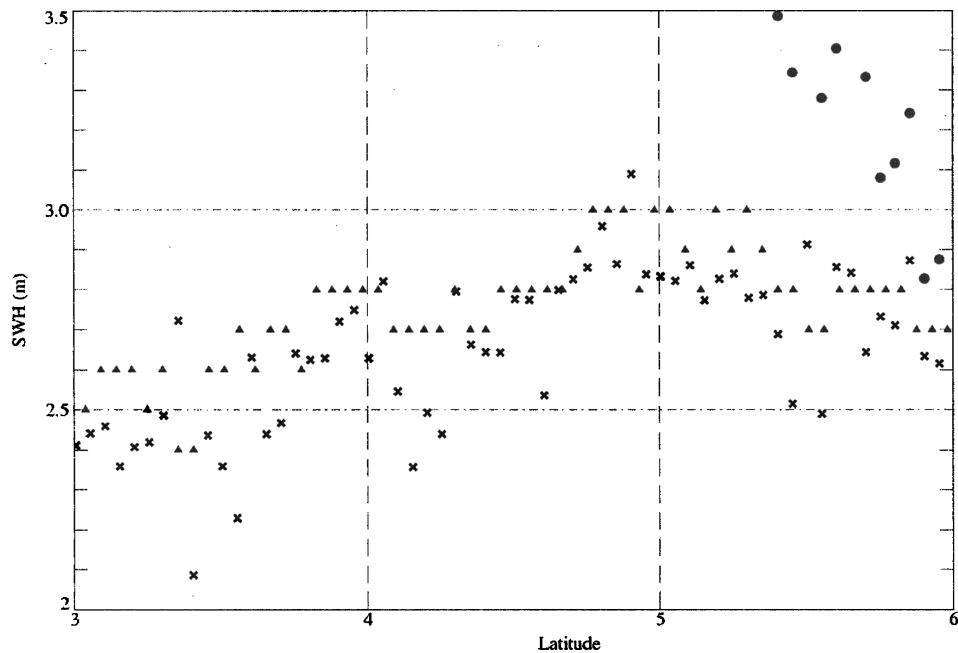


**FIGURE 13b** Significant wave height (zoom on the previous plot): MLE3 (bullets), MLE4 (crosses) and Topex (triangles) (first star tracker incident: 04/04/2002—Cycle 008 (Jason-1)—pass 252).

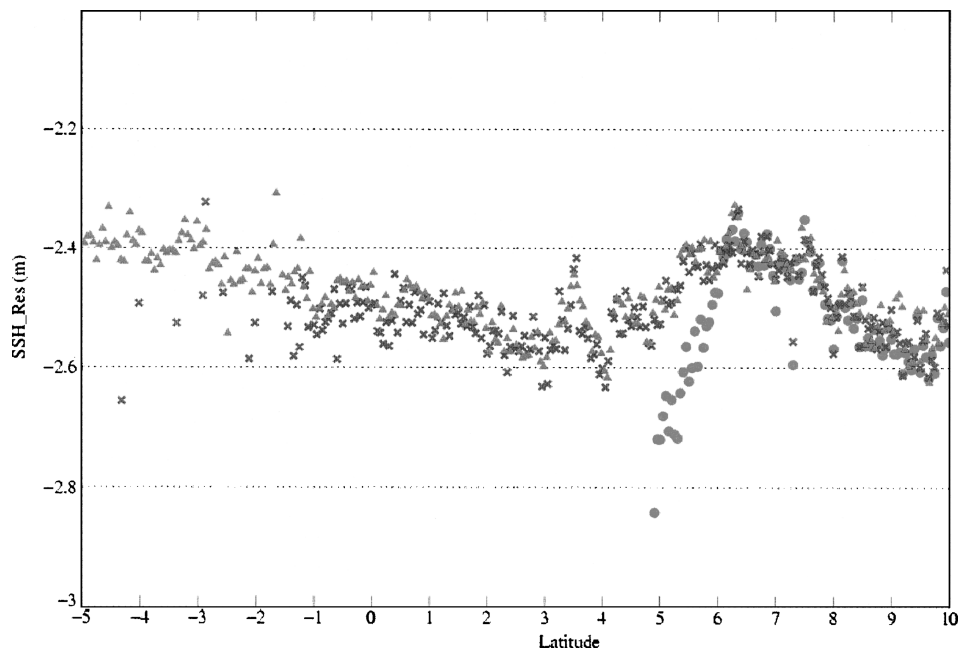


**FIGURE 14a** Sea Surface Height Residuals: MLE3 (bullets), MLE4 (crosses) and Topex (triangles) (first star tracker incident: 04/04/2002—Cycle 008 (Jason-1)—pass 252).

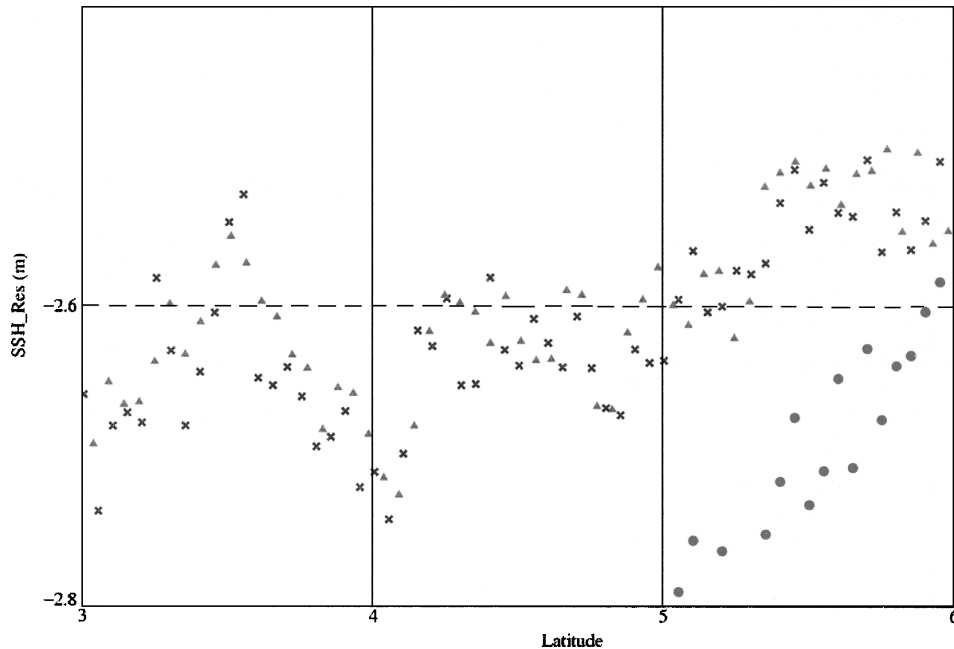


**FIGURE 14b** Sea Surface Height Residuals (zoom on the previous plot): MLE3 (bullets), MLE4 (crosses) and Topex (triangles) (first star tracker incident: 04/04/2002—Cycle 008 (Jason-1)—pass 252).

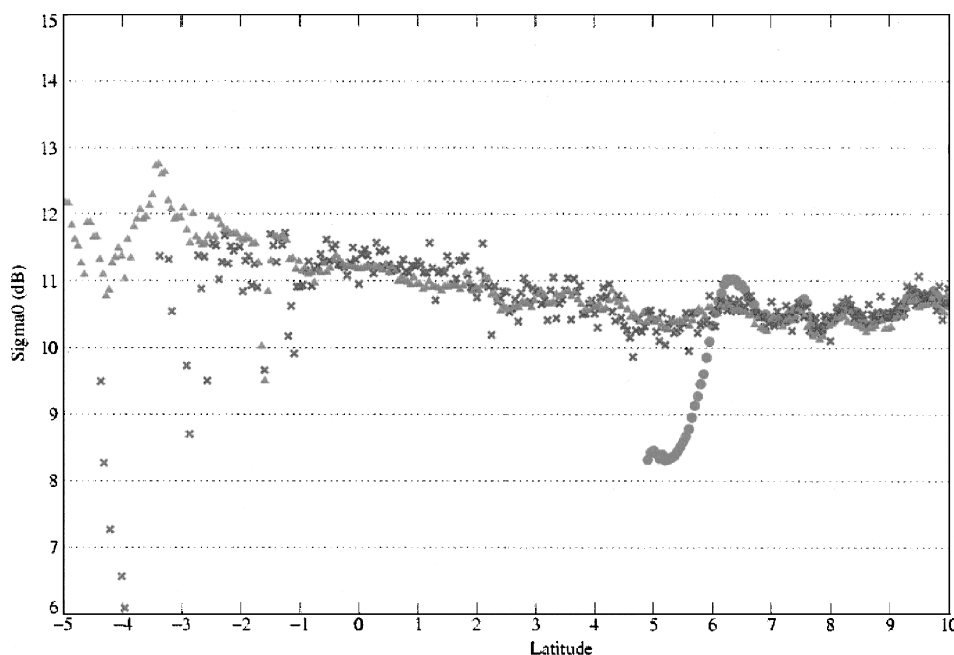


**FIGURE 15a** Sigma 0 coefficient: MLE3 (bullets), MLE4 (crosses) and Topex (triangles) (first star tracker incident: 04/04/2002—Cycle 008 (Jason-1)—pass 252).

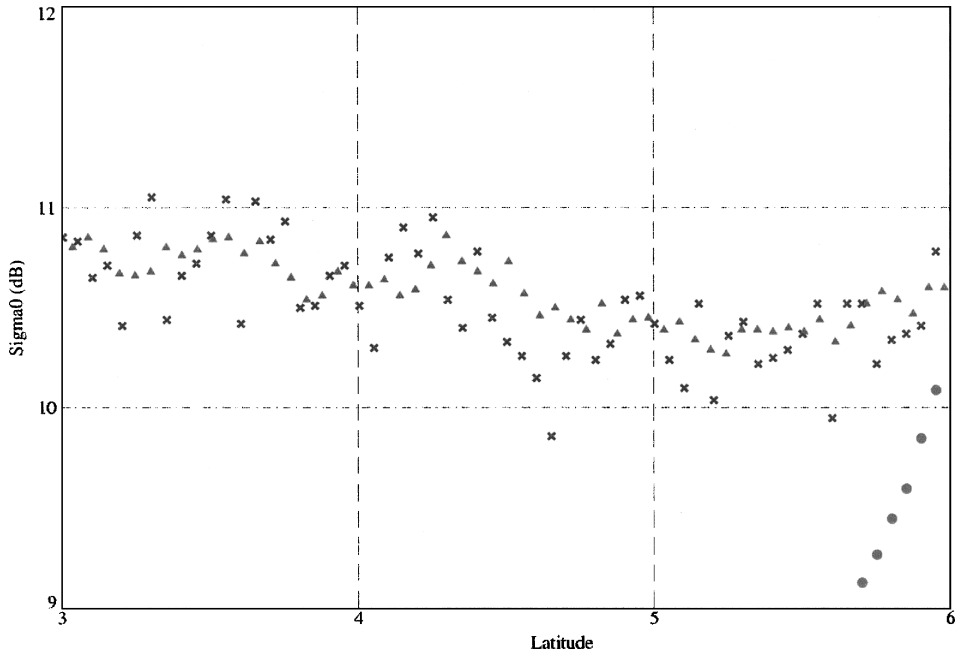


**FIGURE 15b** Sigma 0 coefficient (zoom on the previous plot): MLE3 (bullets), MLE4 (crosses) and Topex (triangles) (first star tracker incident: 04/04/2002—Cycle 008 (Jason-1)—pass 252).

performance section, the range parameter is overestimated for MLE3. This is in agreement with the MLE3 SSH residuals (*Orbit-Range\_Ku-Mean\_Sea\_Surface*) being underestimated when the attitude angle increases. The backscatter coefficient is underestimated. On the other hand, MLE3 significant wave heights are overestimated.

The MLE3 estimates (i.e., GDR products) are not available for mispointing angles greater than 0.3 degree. For such angles ( $>0.3$  degree) the MLE3 retracking algorithm does not converge. Looking at Figure 16, this appears to be a nonfrequent situation even for cycles 35 and 36 that are affected by the anomalous behavior of the star tracker. Indeed, from the beginning of the mission, the mean value of the square of the off-nadir angle has been equal to  $-4.17 \times 10^{-3}$  squared degrees, whereas its standard deviation is equal to  $1.65 \times 10^{-3}$  squared degrees.

On the other hand, for all attitude angles from 0 to 0.8 degree, the MLE4 algorithm fully converges. The geophysical results are consistent with TOPEX results which are not corrupted by irregular mispointing angle of the TOPEX/Poseidon platform. The agreement (for all parameters) between MLE4 outputs and TOPEX measurements is near perfect.

The next section shows a complete validation of these results based on a larger amount of data (several cycles of data).

#### Evaluation Based on Several Cycles of Data

Figure 17 shows the mean of the attitude angle per pass for cycles 35 and 36 (resp. a and b) (as issued from the GDR products). In these plots, we can see that the off-nadir angle is higher than its usual value during the second half of cycle 35 and the first half of cycle 36: This is due to star tracker problems. This period (from pass 121, Cycle 35 to pass 120, cycle 36) gives us a good opportunity to validate the new algorithm and to perform

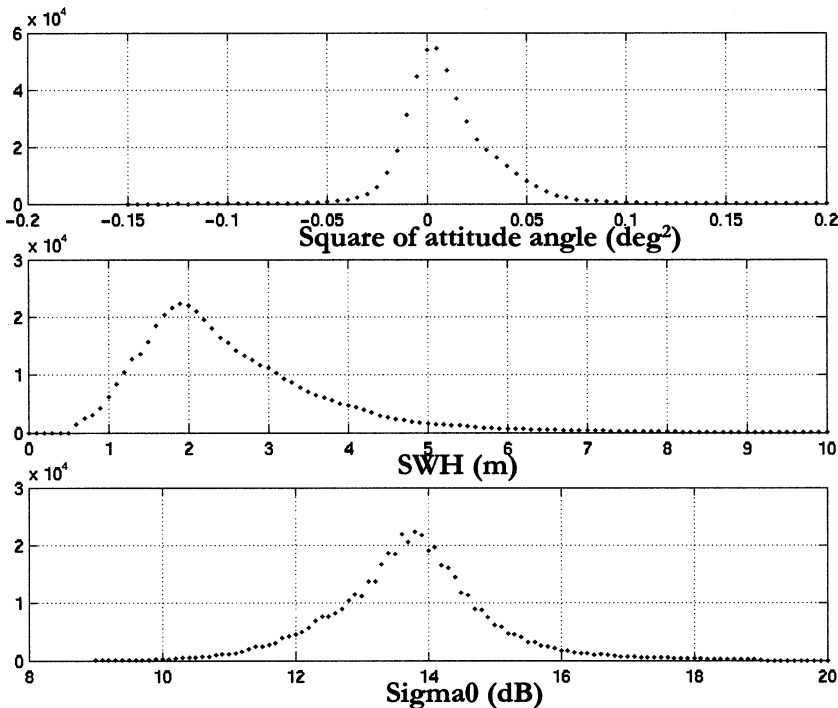


**FIGURE 16** Histogram of (a) Off-nadir angle (MLE4), (b) SWH and (c) Backscatter Coefficient for the MLE4 algorithm—Cycle 35–36.

a statistical analysis of the impact of the new algorithm, based on a significant amount of data.

#### General Statistical Results

Table 1 displays the mean and standard deviation of each parameter for both algorithms. Results for both algorithms are really close. The addition of a fourth parameter in the retracking algorithm leads to a very small increase of the noise level on the range. This is in line with the theoretical performances observed in the previous section. Figure 18 (resp. 16) shows the histograms of the main parameters for the MLE3 (resp. MLE4) solution. Histograms are very similar except for the mispointing angle. The mean

**TABLE 1** Comparison of Mean and Standard Deviation Levels on Cycles 35–36 and 61

		Cycle 35–36 MLE3	Cycle 35–36 MLE4	Cycle 61 MLE3	Cycle 61 MLE4
Range	rms (cm)	7.3900	7.9800	7.3400	7.9400
SWH	Mean (m)	2.5700	2.5460	2.5300	2.4900
	rms (m)	0.5330	0.5370	0.5470	0.5480
Sigma0	Mean (dB)	13.7250	13.7300	13.8100	13.8500
	rms(dB)				
Square of	Mean ( $\text{deg}^2$ )	0.0036	0.0112	-0.0060	0.0030
mispoint. angle	rms( $\text{deg}^2$ )	0.0273	0.0244	0.0014	0.0015
Nb of valid pts/sec	Mean (/)	19.5000	19.4800	19.5800	19.5200

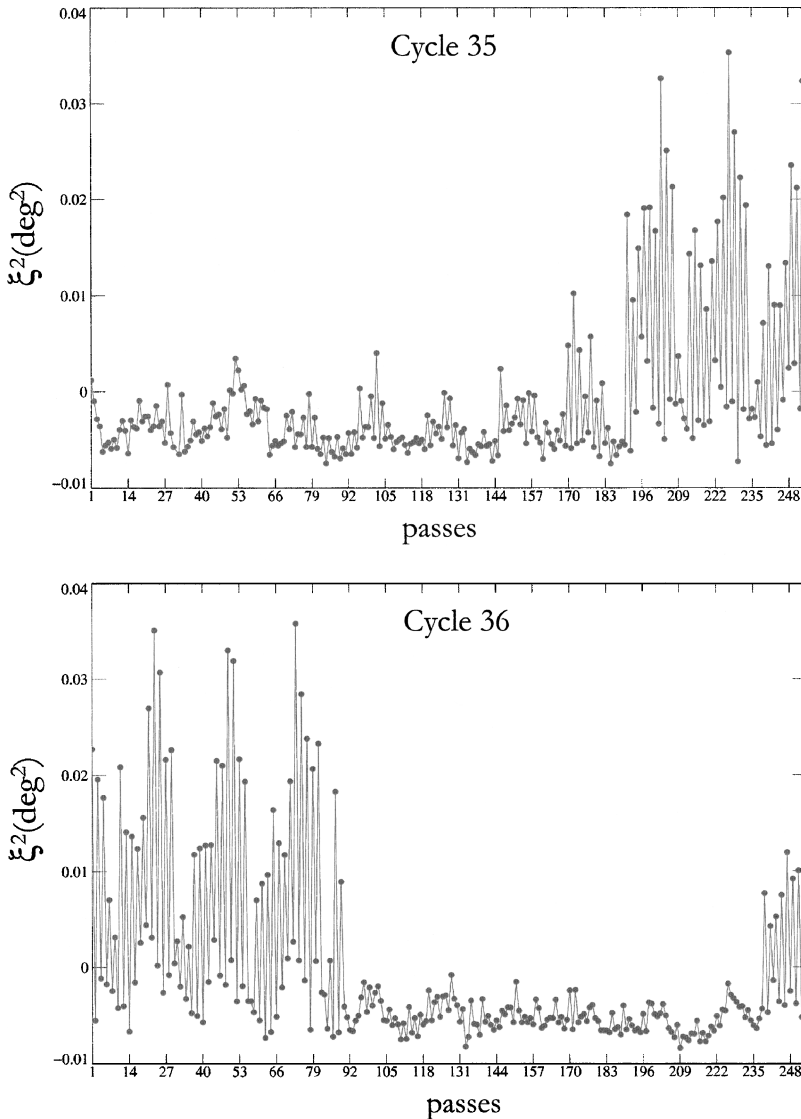


**FIGURE 17** Mean of the square of the attitude angle by pass—Cycles 35 and 36.

cycle value of this parameter is positive in the MLE4 case while it is slightly negative for the MLE3 case. We can then conclude that the linear regression on the trailing edge used to deliver the attitude angle available in the GDR products, gives slightly biased estimates. Fitting the whole waveform to the model provides improved unbiased results. The variance of the mispointing angle parameter is also reduced when using the MLE4 algorithm.

Let's now try identifying possible dependencies of the sea surface height on mispointing angle, significant waveheight, or backscatter coefficient.

In Figure 19, the first row displays the number of measurements taken into account per SWH and  $\xi^2$  box (box width for SWH: 10 cm and for  $\xi^2$ : 0.005 degrees<sup>2</sup>). The second row shows the sea surface height residual plotted versus SWH and the square of the off-nadir angle.

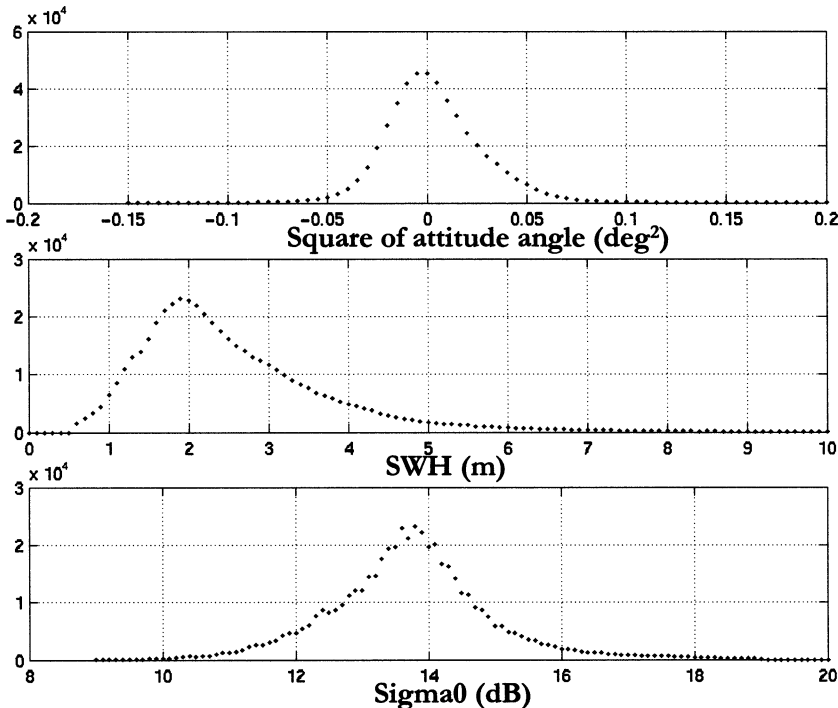


**FIGURE 18** Histogram of (a) Off-nadir angle (linear regression), (b) SWH and (c) Backscatter Coefficient for the MLE3 algorithm—Cycle 35–36.

Figure 20 plots the same parameter as a function of SWH and backscatter coefficient (box width for SWH: 10 cm and for Sigma0: 0.1 dB). MLE3 and MLE4 plots are really close. This shows that the new algorithm has negligible impact on the dependencies of the residual measurements. Moreover, the sea state bias, the pseudo time tag bias issued from crossover analysis and the sea surface height crossover residuals are reduced (see Table 2).

#### Comparisons with Cycle 61 Results

In the previous section, results have been displayed and analyzed for a specific 10-day period having a large amount of attitude data out of the specification. Let's now analyze the results obtained for a typical cycle (cycle 61). Figure 21 displays the mean pass per pass value, of the square of the off-nadir angle. It appears again that, whereas the mean value is negative in the MLE3 panel, it is positive in the MLE4 one ( $2.7 \times 10^{-3}$

**TABLE 2** Statistical Validation on Cycle 35–36

	Cycle 35–36—MLE3	Cycle 35–36—MLE4
SSH crossover residuals (cm)	6.253	6.123
Time tag bias (ms)	0.061	0.037
Electromagnetic bias (%SWH)	4.155	4.04

The SSH crossover residuals are computed with the following editing criteria: bathymetry lower than -1000m, latitudes varying from -50° to +50°, oceanic variability lower than 20 cm.

The time tag bias has been computed at the crossover points.

The electromagnetic bias is obtained with the BM1 solution.

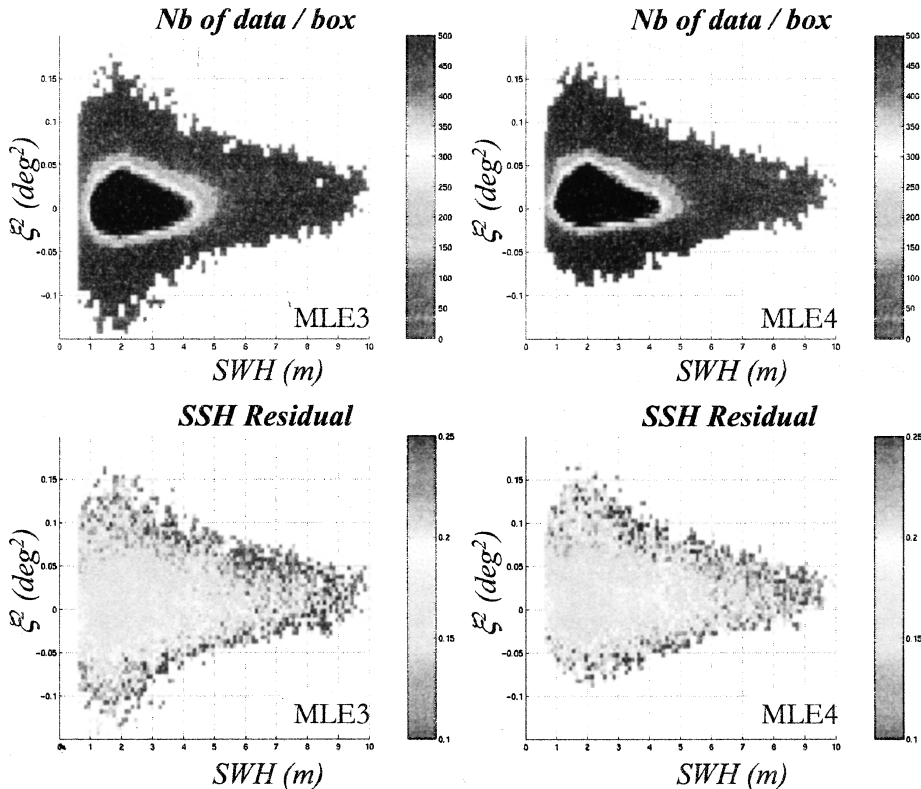


**FIGURE 19** Dependencies of the sea surface height residual with SWH and square of the off-nadir angle for cycle 35–36.

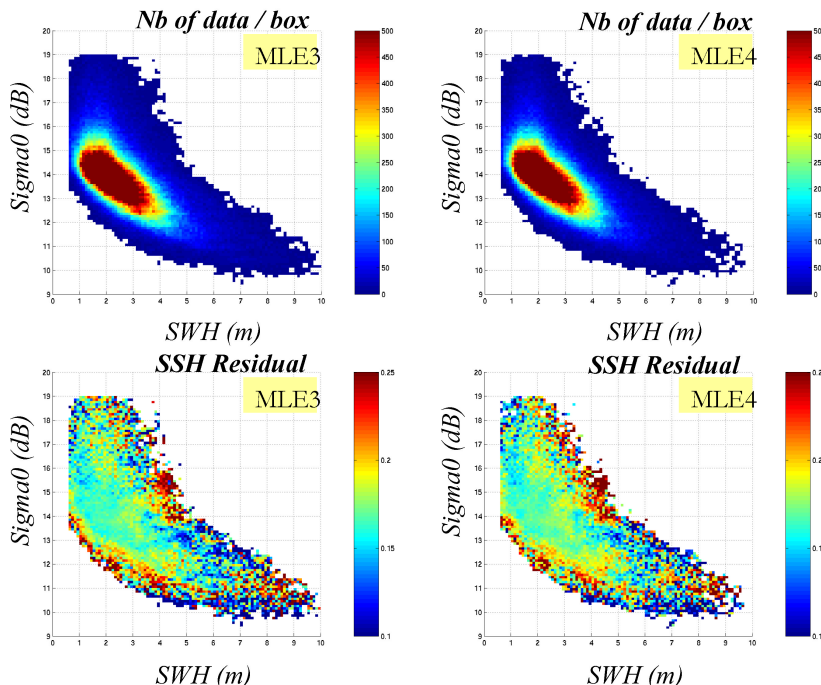


**FIGURE 20** Dependencies of the sea surface height residual with SWH and backscatter coefficient for cycle 35–36.

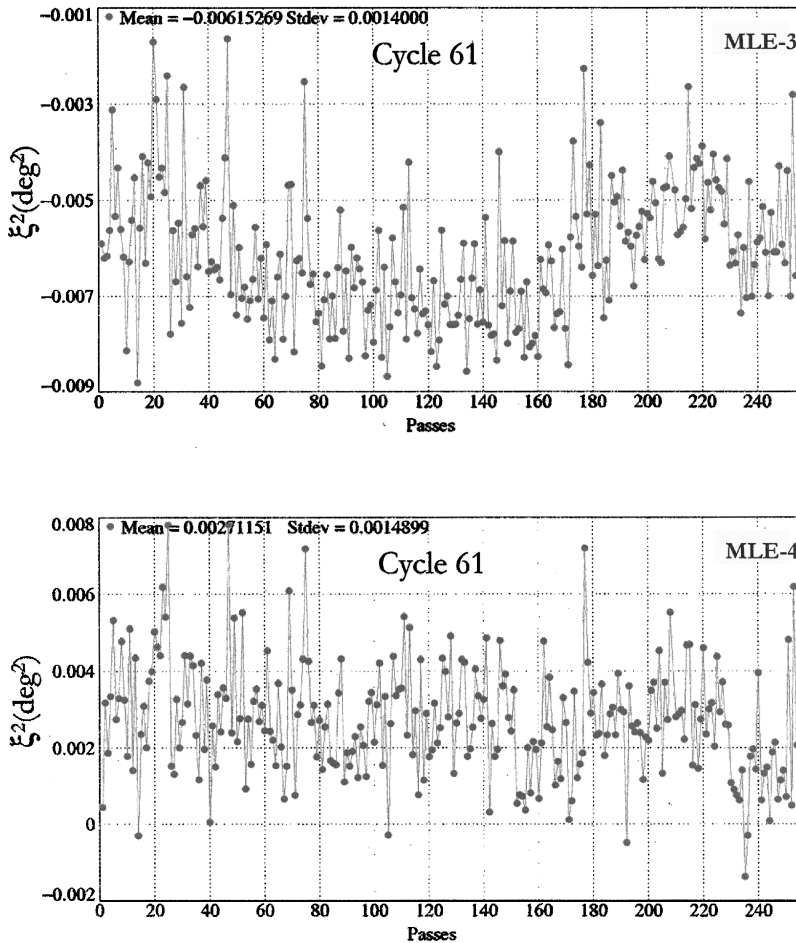


**FIGURE 21** Mean of the square of the attitude angle by pass—Cycle 61 obtained by MLE3 and MLE4 retracking algorithm.

$\text{deg}^2$ , leading to a 0.05 deg for  $\xi$ , corresponding to the performance derived from AOCS measurements).

As shown for cycles 35–36, the sea state bias, the pseudo time tag bias issued from crossover analysis and the sea surface height crossover residuals are detailed in Table 3.

**TABLE 3** Statistical Validation on Cycle 61

	Cycle 61—MLE3	Cycle 61—MLE4
SSH crossover residuals (cm)	6.168	5.74
Time tag bias (ms)	0.263	0.256
Electromagnetic bias (%SWH)	3.557	3.578

The SSH crossover residuals are computed with the following editing criteria: bathymetry lower than -1000m, latitudes varying from  $-50^\circ$  to  $+50^\circ$ , oceanic variability lower than 20 cm.

The time tag bias has been computed at the crossover points.

The electromagnetic bias is obtained with the BM1 solution.

## Conclusions and Perspectives

To mitigate the consequences of a possible further degradation of the Jason-1 star trackers performances on the estimated ocean parameters, we have presented a new method to estimate the ocean parameters in the case of high values of the mispointing angle. This new method is based on a second order model of the altimeter waveform and a 4-parameter maximum likelihood estimator.

After a brief review of the Poseidon-2 altimeter characteristics and a brief description of the MLE3 algorithm operationally used in the ground processing to estimate the parameters, a second order model of the waveform has been introduced. This model clearly helps handling higher values of the mispointing angle (up to  $0.8^\circ$ ). It is used jointly with the Maximum Likelihood Estimator to estimate all the geophysical parameters. The performances of this method have been evaluated theoretically using simulated waveforms and have been compared to the MLE3 method used in the operational ground processing.

As expected, both estimators are comparable for small mispointing angles ( $<0.3^\circ$ ). Beyond this limit and up to 0.8 degree, the highest quality of the proposed method has been demonstrated. The conclusion is still valid when processing real data acquired by the Jason-1 satellite during the period when TOPEX and Jason-1 were flying on the same ground track.

The results provided in here concern the Ku-band data only. An adaptation of this method is under testing on the C-band data, taking benefit from the findings of this study.

## References

- Abramowitz, M., and I. A. Stegun, (Eds.). 1972. *NBS Handbook of mathematical functions*. New York: Dover.
- Amarouche, L. 2001a. *Contribution à l'Etude du Biais d'Etat de Mer*. PhD Thesis from Université Paris VII, Paris, France.
- Amarouche, L., E. Thouvenot, B. Chapron, and O.-Z. Zanifé. 2001b. *A New Estimator of the Sea State Bias using a Three Frequency Radar Altimeter*, IGARSS' 01, Proceedings, Sydney, Australia. 2510–2512.
- Barrick, D. E. 1972. Remote sensing of the sea state by radar. Pp.—in *Remote Sensing of the Troposphere*, V. E. Derr (ed.). Washington, D.C.: U.S. Govt. Printing Office.
- Barrick, D. E., and B. J. Lipa. 1985. Analysis and interpretation of Altimeter sea echo. *Adv. Geophys.* 27:61–100.
- Brown, G. S. 1977. The average impulse response of a rough surface and Its application. *IEEE Transactions on Antenna and Propagation*, Vol. AP. 25, N°, 1, pp. 67–74.
- Carayon, G., N. Steunou, J. L. Courrière, and P. Thibaut. 2003. POSEIDON 2 radar altimeter design and results of in flight performances. *Mar. Geod.* 26(3–4):159–165.
- Chelton, D. B., E. J. Walsh, and J. L. MacArthur. 1989. Pulse compression and sea level tracking in satellite altimetry, *J. of Atmos. and Oceanic Tech.* 6:407–438.
- Desai, S. D., and P. Vincent. 2003. Statistical evaluation of the Jason-1 operational sensor data record. *Mari Geod.* 26(3–4):187–199.
- Dumont, J.-P. 1985. *Estimation Optimale des Paramètres Altimétriques des Signaux Radar Poseidon*. PhD Thesis from Institut National Polytechnique de Toulouse, Toulouse, France.
- Hayne, G. S. 1980. Radar altimeter mean return waveforms from near-normal-incidence ocean surface scattering. *IEEE Transactions on Antennas and Propagation* AP-28(5):687–692.
- MacArthur, J. L. 1978. Seasat, a radar altimeter design description, Rep. SDO-5232. *Appl. Phys. Lab.*: Johns Hopkins Univ., Baltimore, Md., 1978.
- Ménard, Y., L. L. Fu, P. Escudier, B. Haines, G. Kunstmann, F. Parisot, J. Perbos, P. Vincent, and S. Desai. 2003. The Jason-1 mission. *Mar. Geod.* 26(3–4):131–146.
- Moore, R. K., and C. S. Williams, Jr. 1957. Radar terrain return at near-vertical incidence. *Proc. IRE* 45(2): 228–238.

- Perbos J., P. Escudier, F. Parisot, G. Zaouche, P. Vincent, Y. Ménard, F. Manon, G. Kunstmann, D. Royer, and L. L. Fu. 2003. Jason-1: Assessment of the system performances. *Mar. Geod.* 26(3–4):147–157.
- Rodriguez, E. 1988. Altimetry for non-Gaussian oceans: Height biases and estimation of parameters. *J. Geophys. Res.* 93:14107–14120.
- Rodriguez E., and J. M. Martin. 1994. Correlation properties of ocean altimeter returns. *IEEE Transactions on Geoscience and Remote Sensing* 32(3): 553–561.
- Walsh E. J. 1982. Pulse-to-pulse correlation in satellite altimeters. *Rad. Sci.* 17(4):786–800.
- Yaplee, B. S., A. Shapiro, D. L. Hammond, B. D. Au, and E. A. Uliana. 1971. Nanosecond radar observations of the ocean surface from a stable platform. *IEEE Trans. Geosci. Electron.* GE-9:170–174.
- Zanifé, O.-Z., P. Vincent, L. Amarouche, J.-P. Dumont, P. Thibaut, and S. Labroue. 2003. Comparison of the Ku range noise level and the relative sea state bias of the Jason-1, topex and poseidon-1 radar altimeters. *Mar. Geod.*, 26(3–4):201–238.